Available online at www.sciencedirect.com
ScienceDirect
Journal of Power Sources 159 (2006) 533–542
JOURNAL OF POWER SOURCES
www.elsevier.com/locate/jpowsour

Automotive composite fuel cell bipolar plates: Hydrogen permeation concerns☆

Richard Blunk[a,*], Feng Zhong[a], John Owens[b]

[a] General Motors Fuel Cell Activities, General Motors Corporation 480-102-000, 30500 Mound Road, Warren, MI 48090, USA
[b] General Motors R&D Center, USA

Received 16 September 2005; accepted 30 September 2005
Available online 24 January 2006

Abstract

At present proton exchange membrane (PEM) performance levels and fuel cell stack operating conditions, require a plate area specific resistance of less than 30 m ohm cm^2 and a plate thickness of less than 2 mm are required to meet the vehicular volumetric power density target (>2 kW l^{-1}). Unfortunately, it is difficult to meet these targets, and simultaneously obtain good mechanical properties and low through-thickness hydrogen permeation rates when using polymeric plate materials. Polymers are brittle at the high conductive filler concentrations (e.g. >50 v/o graphite) required for high conductivity, and are more likely to generate high convection-driven H_2 permeation rates at a high graphite loading and at a thin plate thickness. As a result, high scrap rates are realized during plate manufacturing and stacking operations, and excessive permeation rates are anticipated in pressurized stacks. This study addresses H_2 permeation concerns associated with using thin, highly-filled composite plates, and investigates factors affecting permeation such as plate temperature, thickness, graphite loading, and aging.

Keywords: Automotive composite fuel cell; Bipolar plates; Hydrogen permeation

1. Introduction

In proton exchange membrane (PEM) fuel cells, chemical energy is converted directly into electrical energy and is not limited by Carnot-cycle constraints; thus, at standard operating temperatures, the thermodynamic efficiency limit of a fuel cell engine is approximately twice that of an internal combustion (heat) engine. In practice, however, voltage losses or overpotentials exist during the low-temperature operation of PEM fuel cells, reducing this efficiency advantage. These losses include: (1) activation losses—slow reaction kinetics in the cathode catalyst layer; (2) mass-transport (gas and protons) losses—failure to transport sufficient reactant to the electrodes; and (3) ohmic losses—low protonic and electronic conduction through the thickness of the polymer electrolyte and the bipolar plate, respectively [1]. As a result of these irreversible losses, which are directly proportional to the stack's operating current density, some chemical energy is converted to thermal energy (heat), requiring the cells to be cooled to prevent thermal runaway and damage to stack components.

A stack volumetric power density greater than 2 kW l^{-1} is required for PEM fuel cells to be viable in vehicle applications. Although large cathodic activation overpotentials (300–400 mV at 1 A cm^{-2}) currently exist and are contributing most to the total losses, not much improvement has been made over the past forty years in reducing these losses. High-temperature membrane studies have only recently been initiated in an attempt to reduce these losses. Likewise, an increased focus on new polymer electrolyte materials has only recently begun in an attempt to increase the membrane protonic conductivity at reduced relative humidity. Instead, to achieve 2 kW l^{-1} in the near future, many fuel cell manufacturers and plate suppliers have focused on reducing the losses attributed to the bipolar plate, namely reducing the mass-transport losses via an optimization in the flow field geometry and plate surface energy, and reducing the ohmic losses via a reduction in the plate thickness and resistivity.

At present membrane electrode assembly (MEA) performance levels and stack operating conditions, a plate area spe-

☆ This paper was published by SPE at the 2005 Automotive Composities Conference and Exposition.

* Corresponding author. Tel. +1 586 9861967; fax +1 586 9862244.
E-mail address: rick.blunk@gm.com (R. Blunk).

0378-7753/$ – see front matter © 2005 Elsevier B.V. All rights reserved.
doi:10.1016/j.jpowsour.2005.09.068

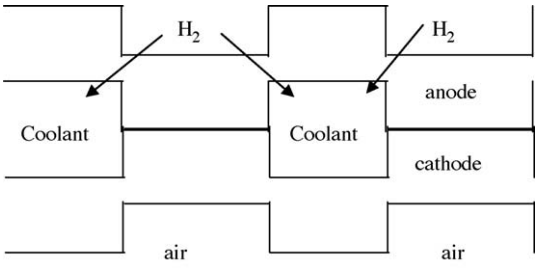

Fig. 1. Schematic of H_2 permeation into bipolar plate coolant (cross-sectional view).

cific resistance of less than approximately 30 m ohm cm^2 and a plate thickness of less than 0.2 cm (<0.03 cm web thickness) are required to achieve the power density target. In addition, at these plate resistance and thickness levels, the rate of hydrogen permeation through the anode plate thickness and into the liquid coolant (see Fig. 1) must not exceed 2.1×10^{-8} cm^3 cm^{-2} s^{-1} (<10 cm^3 h^{-1} $stack^{-1}$, 52 kPag H_2, 90 °C) to prevent hydrogen build-up to unsafe concentrations (>2% v/o) and to preclude insulating H_2 bubbles from accumulating in relatively stagnant coolant channels, resulting in poor heat rejection, hot spots, and premature thermally-induced MEA failures. Suppliers are attempting to meet these resistance, thickness, and permeation requirements using both metal and polymer plates.

Metal plates such as titanium and stainless steel possess excellent mechanical and gas permeation attributes, enabling thin plates (~0.01 cm web thickness) to be manufactured at high dimensional tolerances, at low scrap rates, and with zero hydrogen permeation rates. And with recent MEA technologies and corresponding low fluoride release rates (i.e. low fluoride concentrations), these metals are anticipated to exhibit acceptable corrosion resistance in a PEM fuel cell environment because a stable and protective metal oxide film (i.e. a passive film) forms on their surfaces [2]. To make these plates conductive, the electrically insulating oxide film must be removed or its thickness reduced (via cathodic cleaning or chemical etching), and a conductive coating must then be applied to prevent growth of the oxide film. Coating imperfections such as pin holes, which expose the metal surface to the fuel cell environment, are not problematic because these passivated pin-hole areas are electrochemically stable and represent only a small fraction of the total area for electron transport. Fuel cell suppliers have developed such protective and conductive inorganic [3] and organic [4] coatings, and continue to conduct long-term electrochemical stability studies within stacks to better assess plate life.

In contrast, polymer plates, for the most part, exhibit excellent stability in the aggressive PEM fuel-cell environment and long-term electrochemical durability is not a concern [5]. It is, however, much more difficult to meet the resistance and thickness targets, and simultaneously obtain good mechanical properties and low permeation rates when using polymer plates. The intrinsically insulating polymer resin must be filled with high loadings (>50 v/o) of corrosion-resistant conductive particles such as carbon black and/or graphite in order to meet the resistance target. These loadings greatly exceed percolation threshold concentrations (5–20 v/o) and approach or surpass critical pigment volume concentrations CPVC (50–70 v/o) used to formulate "electrically-conductive" plastics and coatings [6]. At the percolation threshold concentration, an interconnecting path of conductive graphite particles forms and extends through the entire sample thickness, enabling electrons to "percolate", i.e. the electrical resistance decreases by many orders of magnitude as the material goes through an insulator–conductor transition. At higher graphite loadings such as that at the CPVC, not enough polymer binder is present to fill the interstices between graphite particles, and many more percolation pathways form for enhanced conductivity, but at the expense of a porous and weaker material [7]. As a result, highly-graphite-filled composite plate materials are currently extremely brittle (<0.4% tensile strain at break) and, depending on whether local graphite concentrations exceed the CPVC, are more likely to be permeable to gases.

Many studies have been conducted with the intent of reducing the percolation threshold so that high material toughness and high conductivity can be achieved. Factors such as binder type, filler particle size/distribution [8], degree of mix [6], polymer blends [9], polymer crystallinity [10], particulate polymer microstructure [12], and filler alignment [11], and their effect on percolation threshold were investigated. Although these studies were successful in reducing the percolation thresholds and in developing materials with resistivities sufficient for antistatic (10^{12} ohm cm), electrostatic painting (10^6 ohm cm), and electromagnetic interference shielding (10^1 ohm cm) applications, these materials are not conductive enough for plate applications (10^{-2} ohm cm). In a more recent study, less than 20 v/o of large chunks (0.05–0.15 cm) of expanded graphite were incorporated into a vinyl ester thermosetting resin and cured, and the conductivity target was met. Unfortunately, the material exhibited poor strength and failed cohesively within the graphite particles and excessive graphite-to-resin phase separation occurred during molding at the required high shear rates [13]. Consequently, separator plates (0.1–0.3 cm thickness) are presently formulated at graphite (not expanded graphite) levels well beyond these percolation levels for conductivity but slightly below the CPVC to achieve adequate strength, flow, and gas impedance. Note that above the CPVC, the material has insufficient carrier polymer and behaves solid-like; consequently, the material does not flow and fill the mold well.

In this study, we assess whether the plate resistance, thickness, and permeation rate targets can be achieved simultaneously using high-graphite-filled composites. We investigated experimentally the impact of high graphite loadings (approaching the CPVC) on H_2 permeation rates, particularly at the desired thin web thicknesses. We also investigated other permeation factors such as temperature, H_2 pressure, and plate aging in order to obtain more insight into the permeation mechanism—convection-driven versus diffusion-driven.

2. Theory

2.1. Charge transport

Fourier's law describes charge transport via conduction (*diffusion*) according to the one-dimensional differential equation:

$$j_e = -k_e \frac{d\phi}{dx}, \quad (1)$$

in which the charge flux j_e is proportional to an electrical conductivity k_e times a negative gradient of an electrical potential driving force ($d\phi/dx$). The conductivity k_e is a material property that depends on the number of charge carriers and the mobility of these carriers, and its magnitude can change 15–18 orders of magnitude from insulators (e.g. plastics) to conductors (e.g. metals). In graphite-filled composite plate materials, electron transport occurs solely through discrete networks of graphite particles ($k_e \approx 10^3$ S cm^{-1}), not through the continuous polymer medium ($k_e \approx 10^{-15}$ S cm^{-1}). Some electron "hopping" or "tunneling" can occur, however, between graphite particles separated by sufficiently thin polymer gaps [6]. In PEM fuel cells, electrons form in the anode electrode via the H_2 oxidation reaction, conduct through the thickness of the bipolar plate, and participate in the cathode electrode via the O_2 reduction reaction.

2.2. Mass transport (diffusion)

Likewise, Fick's law describes mass transport via conduction (*diffusion*) according to the one-dimension differential equation:

$$j = -DS\frac{dp}{dx} = -P\frac{dp}{dx}, \quad (2)$$

in which the mass flux j is proportional to the conductivity or permeability P of the medium times a negative gradient of a pressure (concentration) potential driving force (dp/dx). In actuality, the driving force is the chemical potential gradient, but for ideal gases such as H_2 that do not interact with the solid phase, the partial pressure p is nearly equivalent to the chemical potential. The permeation coefficient is the product of the diffusion coefficient D and the solubility coefficient S, and is a function of the chemical structure and the morphology of the polymer, as well as many other factors such as temperature and humidity (see Table 1 for general trends of permeability).

Table 1
Gas permeation in polymers: rate as a function of increasing factor

Factor	Permeation rate
Density	Decrease
Crystallization	Decrease
Molecular weight	Little effect
Orientation	Decrease
Cross-link density	Decrease
Filler concentration	Decrease
Humidity	Increase
Temperature	Increase
Plasticizer	Increase

The solubility coefficient relates the concentration of the solute (H_2) in the gas phase p_1 to its concentration in the solid phase c_1 at the gas/solid interface under equilibrium conditions (i.e. $c_1 = S \times p_1$).

Molecular H_2 permeation occurs primarily through the polymer phase of composite plate materials, not through the dense graphite particles, due to the high level of molecular motion found in polymers. Free volume theory indicates that polymer chain segmental motion creates "holes" for penetrant to migrate. The transport of a penetrant through a homogeneous medium, in the absence of gross defects such as pores or cracks, is usually considered to occur by the following three steps: (1) solution (condensation and mixing) of the gas in the surface layers; (2) migration or diffusion of the penetrant to the opposite surface under a concentration (chemical potential) gradient; and (3) evaporation from that surface into the ambient phase. The migration of the penetrant can be visualized as a sequence of unit diffusion steps or jumps from one free volume to the next. For a polymer above its glass temperature, as in simple liquids, fluctuations in density of "holes" are constantly disappearing and reforming as a result of thermal fluctuations.

Gross defects, such as pinholes and cracks, cause a material to leak profusely due to convection, not diffusion. It is the smaller defects which give more subtle, but important, contributions to the overall transport and solution processes, and are of interest here. These include spherulitic and lamellar boundary regions in semi-crystalline polymers and permanent or transient voids (e.g. excess free volume, "frozen holes") found in glassy polymers and, in our case, found in thin, high-graphite-filled polymers near the CPVC.

2.3. Mass transport (convection)

Alternatively, d'Arcy's law describes mass transport via *convection* in porous media according to:

$$j = \frac{-\Delta p}{L\mu} \underbrace{\frac{D_p^2 \varepsilon^3}{150(1-\varepsilon)^2}}_{\kappa} = -\frac{\kappa}{\mu}\frac{\Delta p}{L}, \quad (3)$$

in which κ is collectively considered to be another physical property of the porous medium, known as its permeability and is a function of the effective particle diameter D_p of the solid phase and the void fraction ε, not occupied by particles [14]. The differential form of d'Arcy's law in one dimension is:

$$j = -\frac{\kappa}{\mu}\frac{dp}{dx}, \quad (4)$$

in which the flux j is proportional to a conductivity (κ/μ) times a negative gradient of a pressure potential driving force (dp/dx). Note that p represents mechanical pressure, not partial pressure, and should not be confused with species concentration nor species chemical potential. For example, in d'Arcy's equation, a mechanical pressure head (pressure gradient), which can be formed by a pump, a hydrostatic head, or a capillary medium, generates fluid flow and, as a result, mass is trans-

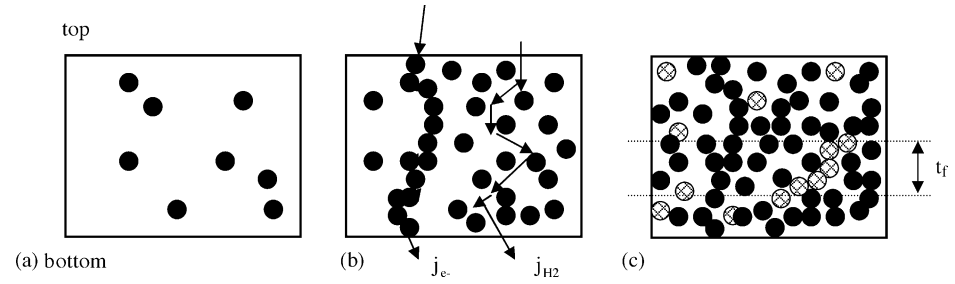

Fig. 2. Proposed H_2 permeation mechanism in polymers as a function of graphite loading (cross sectional view): (a) low graphite, diffusion-driven permeation; (b) graphite at electrical percolation threshold, diffusion-driven permeation; (c) graphite at CPVC, convection-driven permeation at thin plate dimension t_f key: (⊗) void; (●) graphite; (◯) polymer.

ported via convection. Convection-driven mass transport occurs in many chemical processes such as in water treatment operations and in enhance oil recovery processes in which fluid (mass) flows through pores surrounding ion exchange particles and through porous sedimentary rock, respectively. Contrastly, in Fick's equation, a partial pressure (chemical) gradient generates mass transport via diffusion. Convection-driven mass transfer rates are nearly always greater than diffusion-driven rates.

Fig. 2 illustrates the proposed H_2 permeation mechanisms as the graphite concentration in a composite plate is increased intentionally for enhanced electrical conductivity. Permeation proceeds from a slow, diffusion-driven mechanism to a fast, convection-driven one as the graphite concentration increases and the plate thickness decreases. In Fig. 2a, the composite material consists primarily of polymer with a small amount of graphite particles. Here, no voids are present between particles. Permeation occurs solely by molecular diffusion (Brownian motion) through the polymer phase due to a partial pressure or concentration gradient. Unfortunately, electrical transport is also slow at this low graphite loading because an interconnecting percolation path of graphite particles does not exist. The graphite loading is below the percolation threshold. In Fig. 2b, the graphite concentration is increased above the percolation threshold but below the CPVC. The material's electrical resistivity decreases due to the presence of an interconnecting graphite path, but unfortunately, not enough to meet fuel cell composite plate targets. The mass diffusion rate decreases compared with that observed in Fig. 1a due to the higher concentration of the dense graphite particles and, in turn, the increase in tortuosity (large resistive path length). In Fig. 2c, the graphite concentration is increased above the CPVC. Voids are now present because of insufficient polymer to coat the particles. Electrical conductivity increases significantly due to direct graphite-to-graphite particle contact, but the voids reduce the resistance to permeation and, in turn, increase the diffusion-driven permeation rate. However, if the material is inhomogeneous with high local graphite concentrations—due to poor mixing and/or due to graphite/polymer phase separation during high shear molding—and the thickness of the plate material is reduced to t_f, it is likely that a percolation path of voids can form, as shown. Here, a transition from diffusion- to convection-driven transport occurs, resulting in a large increase in the H_2 permeation rate.

3. Experimental

3.1. Electrical resistance measurement method

The resistance of the plate materials should be measured at "stack conditions", namely the sample should contain flow field channels and should be sandwiched and compressed at stack pressures between two pieces of diffusion media (DM), as shown in Fig. 3. The area specific (total) resistance r is the sum of the bulk material resistance and the pressure-dependent contact resistances located at the two DM/plate interfaces, and has units of ohm cm^2. The resistance is measured using a four-point method and calculated from measured voltage drops V and from known applied currents and sample dimensions, as follows:

$$r = \frac{V}{i}, \tag{5}$$

in which i is the current density.

The voltage drop is measured across either the two diffusion media (total resistance) or two points on the plate surface (bulk resistance). For the former, thick DM (1.0 mm, Toray TGP-H-1.0T) is used so that needle-like voltage probes can make contact with the DM easily. The contact resistance is the total resistance less the bulk resistance.

The contact resistance (CR) at the DM/plate interface is significant and typically contributes more to the total plate resistance than the bulk resistance, particularly at low compression pressures. CR is not clearly understood because it depends on so many factors such as bulk conductivity, sam-

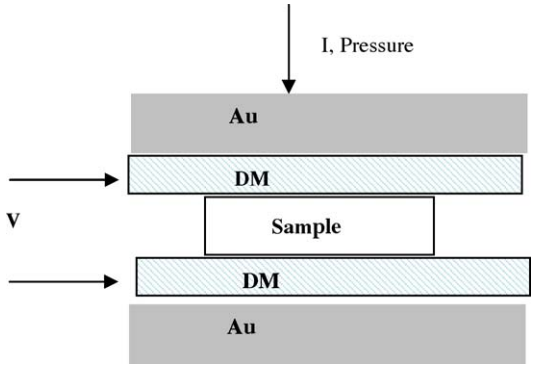

Fig. 3. Schematic of four-point test method for measuring the area specific resistance of materials.

ple flatness and roughness, pressure, and surface composition. It is clear, however, that the CR must be reduced in order to meet the resistance target at low stack compression—needed for reduced mass-transport overpotentials—and at reduced filler loadings—needed for enhanced mechanical properties and reduced H_2 permeation rates. This can be accomplished somewhat by using a more electrically conducting layer, i.e. a conductive-tie layer, at the DM/plate interface that "short circuits" the flow of current from the DM fibers to the conductive particles at the plate surface [15]. Studies have been done using the conductive-tie layer concept (reduce CR) in combination with aligning high-aspect ratio conductive fillers in the through-plane direction (reduce bulk resistance) in an attempt to meet the conductivity target at low loadings. Unfortunately, this target was not achieved, so plate suppliers continue to formulate resins containing high graphite loadings and hope that their inherently brittle materials can be manufactured thin at low scrap rates and survive the mechanical loads in vehicular applications.

3.2. Permeation measurement method

The transmission rate of gas through polymer films is measured using two different methods (ISO 2556). The differential pressure method (or pressure decay/rise method) entails initially pressurizing one side of the sample in the permeation cell with H_2, and measuring the time rate of decrease/increase of pressure on the same/opposite side of the sample. The equal pressure method entails supplying H_2 to one side of the sample, flowing argon carrier gas to the other side under the same pressure, and measuring the transmitted H_2 using a H_2 detector. The latter method is used in this study and is shown schematically in Fig. 4.

H_2 and Ar gases are metered separately through temperature-controlled humidifiers (bubblers), and heated/humidified to preset levels. The conditioned gases are then passed to the heated permeation cell and pressurized to preset levels through the use of pressure regulators. The cell consists of standard fuel cell LANL hardware (Fuel Cell Technologies Inc.) made from graphite with high-pitch flow field channels. Graphite eliminates corrosion problems and the fine channels provide mechanical support to thin/brittle composite plate samples (i.e. reduces sample breakage during gas pressurization) and enables gases to reach the sample surface for permeation. In both compartments of the permeation cell, Toray diffusion medium (TGP-H-1.0T) is sandwiched between the flow field channels and the sample to ensure 100% sample area utilization for permeation. Sample size is 10.2 cm × 10.2 cm and sample permeation area is 50 cm^2. H_2 leaving the cell is vented while the Ar carrier gas, which now contains H_2 that permeated through the sample thickness, is passed through a condenser to remove excessive water before entering the gas chromatograph H_2 detector. The H_2 concentration in the Ar gas stream is a function of the Ar flow rate and the H_2 permeation rate.

The existing equipment can measure H_2 permeation rates accurately down to 3.5×10^{-8} $cm^3\,cm^{-2}\,s^{-1}$, or 1.5 times greater than the permeation target of 2.1×10^{-8} $cm^3\,cm^{-2}\,s^{-1}$. This resolution is sufficient for current composite plate materials and plate thicknesses. H_2 permeation rates can be measured as a function of temperature, H_2 pressure, relative humidity, and sample thickness and composition. Sample pre-soak (aging) effects can also be investigated.

The following test protocol was used to measure the H_2 permeation rates through the thickness of composite plate materials:

- (For aging effect studies only) precondition sample at 90 °C in a fuel cell simulated solution (1.8 ppm HF, 12.5 ppm H_2SO_4, pH 3.0) for preset soak times. Solution migration into the polymer sample may plasticize or "loosen up" the structure, creating more free volume, and in turn, increasing permeation rates.
- Place sample in permeation cell and let it equilibrate overnight for 18 h at 90 °C, 100% RH, and 172.1 kPag (Ar and H_2) to reach maximum and steady-state permeation rate. Based on a "rule-of-thumb" penetration time calculation (sample thickness squared divided by six times the diffusion coefficient), equilibration times ranging from 0.75 to 7.5 h are required for a sample thickness of less than 1 mm [16].
- Measure the Ar flow rate before (mass flow controller) and after (soap film bubble meter) the gas chromatograph (GC).

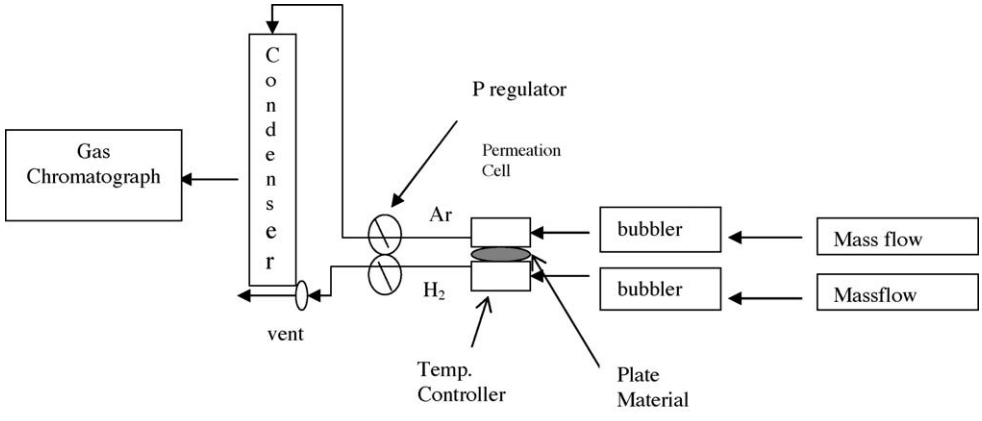

Fig. 4. Schematic of H_2 permeation equipment.

Table 2
Accuracy of H_2 permeation test method

Sample	GM method (cm^3(STP) cm cm^{-2} s Pa)	Other methods (cm^3(STP) cm cm^{-2} s Pa)	Percent difference (%)
Nafion® membrane	1.4×10^{-11}	1.3×10^{-11} electrochemical	+7.7
Teflon® film	2.8×10^{-12}	2.9×10^{-12} pressure rise[a]	−3.4
GE 8010-MC-112 polycarbonate	9.7×10^{-13}	8.0×10^{-13} pressure rise[b]	+21

[a] R.A. Pasternak et al., Macromolecules, 3 (1970) 366.
[b] C. Extrand, Entegris Fuel Cells, Chaska, MN, USA.

Table 3
H_2 permeation rate comparison of fuel cell materials

Material	Thickness (cm)	Equivalent current (mA cm^{-2})	Current normalized to target
Target	0.03	1.81×10^{-4}	1
Composite T	0.03	6.4×10^{-4}	3.5
Composite N	0.03	2.5×10^{-3}	13.8
Composite S	0.03	1.4×10^{-2}	77
Nafion® membrane	0.0025	7.99	44143

The two readings should agree to within 5% to ensure no leakage in the system.

- Inject H_2-containing Ar gas into the GC to determine H_2 concentration. At least three measurements are recommended for confidence in data.
- Change H_2/Ar pressures to 172/137 kPag, wait 2 h for equilibration, and inject Ar gas into GC to determine mass transport mechanism—diffusion- or convection-driven permeation. If a pressure differential cannot be maintained, then the sample contains a pinhole or a crack, H_2 transport is by convection, and the permeation data obtained in the previous step should be discarded. The sample is bad. If a pressure differential is maintained and the data agree with those in the previous step, then permeation is independent on the mechanical pressure head and permeation is solely by diffusion. However, if 172/137 kPag is maintained and the H_2 concentration in the Ar stream increases, then permeation is primarily convection-driven.
- Change H_2/Ar pressures to 137/172 kPag, wait 2 h for equilibration, and inject Ar gas into GC to determine mass transport mechanism—diffusion- or convection-driven permeation. These data will reinforce those from the previous step. If permeation is convection-driven, the concentration of H_2 will decrease significantly with a higher pressure head on the Ar side of the cell.
- Inject calibration gases (10, 100, 500 and 5000 ppm H_2 in Ar) into GC to calibrate GC and to ensure measurement accuracy as GC output may drift with time.
- Calculate H_2 permeation rates, based on Ar flow rate, GC-measured H_2 concentrations, and sample area.

4. Results

Permeation rates of three materials were measured using the equal pressure method described above and the results compared with those obtained internally using an electrochemical technique or externally (from literature) using the pressure rise method. The electrochemical method entails pressurizing one side of a Pt-containing membrane with H_2 and the other side with N_2, applying an anodic potential on the N_2 side, and measuring the H_2 oxidation (permeation) currents attributed to H_2 permeating through the membrane material. The comparison data are tabulated in Table 2. Note that permeation coefficients are used instead of rates to normalize out pressure and thickness differences among the samples. All testing was done at 90 °C. In general, based on the low permeation rates and thus high resolution needed, good agreement was achieved, indicating that the GM permeation method is accurate.

Table 3 lists measured H_2 permeation rates (172.3 kPa, 100% RH, and 90 °C) through the thickness of various molded high-graphite-filled composite plate materials as well as through the fuel cell membrane material. Composite T contains a thermoplastic liquid crystalline resin, whereas composite N and S contain a thermosetting phenolic and vinyl ester resin, respectively. A target thickness of 0.03 cm was used for the composite samples. The rate data are converted into equivalent electrochemical current data to obtain more insight into electrical efficiency losses in an operating fuel cell due to H_2 permeation. The permeation target (<10 cm^3 h^{-1} $stack^{-1}$, 90 °C, 48.2 kPa) is also listed and compared against the sample permeation rates.

The H_2 flux is two–four orders of magnitude greater in the membrane material compared to that in the composite plate material and may contribute to premature electrochemical-induced failures within the membrane. However, the overall magnitude of the membrane permeation (7.99 mA cm^{-2}) is relatively small in comparison with typical operation fuel cell currents (200–1000 mA cm^{-2}), so efficiency losses attributed to membrane permeation are insignificant. The permeation rates for the composite materials exceed the target value at the targeted thickness. However, composite T will meet the target (assuming transport is governed by Fick's law of diffusion) if the measured rates are divided by a factor of 3.5 because the experimental pressure of 172.3 kPa is 3.5 times greater than the target pressure of 48.2 kPa.

The magnitude of the permeation rate target is inversely proportional to the complexity and cost of a system to remove

Table 4
Diffusion- and convection-driven H_2 transport in composite T material (90 °C, 172 kPa H_2, 0.03 cm thickness)

Sample preparation	Permeation rate ($cm^3\ cm^{-2}\ s^{-1}$)		Permeation rate increase with decreasing Ar pressure (factor increase)	H_2 transport mechanism
	172 kPa Ar	137 kPa Ar		
Molded	7.67×10^{-8}	7.43×10^{-8}	−0.97	Diffusion
Molded	3.58×10^{-8}	3.63×10^{-8}	+1.01	Diffusion
Molded	6.43×10^{-7}	5.76×10^{-6}	+9.0	Convection
Ground	2.67×10^{-6}	3.76×10^{-5}	+14.1	Convection
Ground	1.13×10^{-7}	1.04×10^{-7}	−0.92	Diffusion
Ground	8.12×10^{-8}	1.76×10^{-5}	+217	Convection

H_2 from the coolant reservoir. The lower the target magnitude, the higher the system cost. H_2 can enter the coolant loop in three ways: (1) permeation through the anode plate thickness; (2) leakage through the anode gasket surrounding the coolant manifold; and (3) generation due to electrolysis of the aqueous-based coolant at high stack voltages. The latter two means can be controlled effectively by appropriate gasket/sealant design and material selection, and by using an ion exchange bed to maintain a coolant conductivity of less than 30 μS cm^{-1}. Hence, the dominant source of H_2 in the coolant is attributed to permeation through composite plates, particularly thin ones. Note that the current DOE permeation target is 1.7×10^{-2} mA cm^{-2}, which is 94 times greater than the GM target.

The permeation rate for composite T in Table 4 meets the permeation rate target at 0.03 cm web thickness. Unfortunately, the authors have found significant variations in permeation rates for composite T, as shown in Table 4. By reducing the Ar carrier gas pressure from 172 to 137 kPa (gage) and maintaining the H_2 pressure at 172 kPag, in accordance with the test protocol, we observed, in some instances, that the permeation rate increases drastically for both surface ground (aluminum oxide wheel) and molded samples. This violates Fick's law of diffusion in which H_2 transport is governed by the partial pressure gradient of H_2. The H_2 flux should have remained unchanged under constant H_2 pressure conditions even with a reduction in Ar pressure, suggesting that transport is not solely diffusion-driven, but convection-driven at a 0.03 cm thickness. In these instances, H_2 transport should be referred to as "leakage", and not as "permeation". It's not obvious based on the limited data available whether sample preparation (ground versus molded) affects the transport mechanisms and, in turn, the permeation rates. More data are required for statistical determination. Note that for all samples the pressure differential between the two compartments of the permeation cell could be maintained, suggesting that large cracks are not present in the composite samples.

4.1. Thickness effects

Fig. 5 illustrates the effect of sample thickness on permeation rate and its mechanism. Composite T was molded to a 0.2 cm thickness and surface ground to a thickness of 0.03, 0.04, and 0.05 cm using an aluminum oxide wheel. At a fixed sample thickness, permeation measurements were made at decreasing H_2 pressures while maintaining an Ar pressure of 172 kPag. In agreement with Fick's law, and assuming steady state is reached,

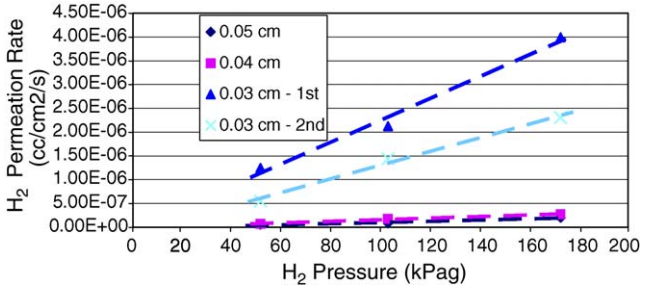

Fig. 5. Effect of thickness on the H_2 permeation rate (composite T material).

the rate of permeation should increase linearly with increasing pressure and approach zero at zero gage pressure. Although the latter is true, the rate increased non-linearly with reduced thickness, as shown in Fig. 5 and more clearly in Fig. 6. A large rate increase was realized between a thickness of 0.04 and 0.03 cm, with significant variation between the two different 0.03 cm thick samples. This indicates that mass transport is diffusion-driven at a large thickness and convection-driven at a small thickness, in agreement with the proposed mechanism illustrated in Fig. 2c. The same trend is also apparent with composite S material, as shown in Figs. 7 and 8. Composite S samples were also molded to a 0.2 cm thickness and surface ground to a thickness ranging from 0.03 to 0.07 cm in increments of 0.01 cm.

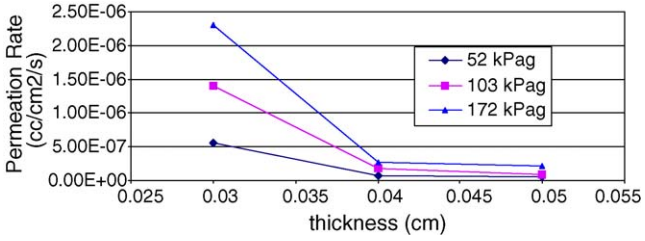

Fig. 6. Effect of thickness on the H_2 permeation rate (composite T material).

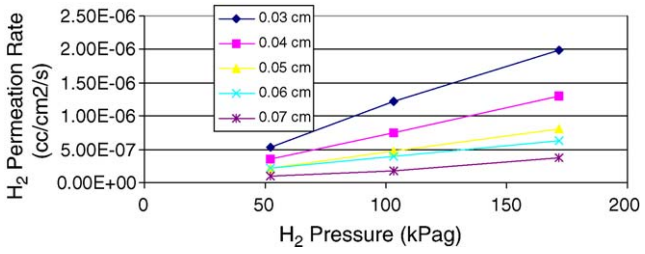

Fig. 7. Effect of thickness on the H_2 permeation rate (composite S material).

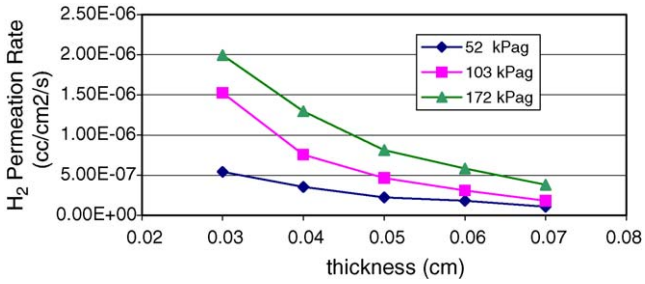

Fig. 8. Effect of thickness on the H_2 permeation rate (composite S material).

4.2. Graphite loading effects

A study was performed investigating the impact of graphite loading on the area specific resistance and the H_2 permeation rate of composite plate materials. UCAR GP195X graphite powder (<50 μm) was dry mixed with Hylar® 461 polyvinylidene fluoride (PVDF) powder in a metallic blender for 1 h at room temperature. For the electrical resistance samples, the mix was compression molded at 4 t to a 0.065 cm thickness using a Parma pellet press to generate the electrical resistance samples (1.3 cm diameter). For the permeation samples (10.1 cm × 10.1 cm area), the powder mix was compression molded at 12 t to a 0.06 cm thickness using an Arber press. High tonnage was used to ensure high densification and, in turn, low resistance and low permeation. The mix was also wet mixed in a Brabender at 200 °C for 15 min followed by compression molding at 195 °C to a 0.065 cm thickness for additional resistance samples. These samples were tested at a compression pressure of 1.4 MPa using the four-point resistance method described earlier. All resistance samples were sanded to remove any insulating polymer-rich surface film.

Electrical resistance results are plotted in Fig. 9. Approximately 65 w/o and 75 w/o graphite is required to achieve the less than 30 m ohm cm^2 resistance target for the dry mix and wet mix samples, respectively. Below 65 w/o graphite, the dry mix samples are significantly more conductive than the wet mix samples, as expected. During wet mixing and below the CPVC, the graphite particles are coated with insulating liquid resin, resulting in a high sample resistance. In contrast, during dry mixing the particles are not completely surrounded by insulating resin, increasing the likelihood of graphite particle contacts and the formation of a percolation network for enhanced conductivity.

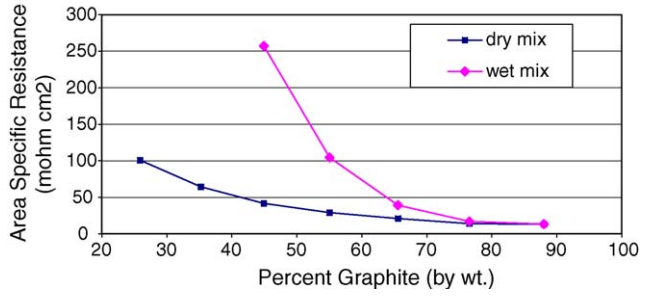

Fig. 9. Effect of graphite concentration on electrical resistance (PVDF/UCAR material).

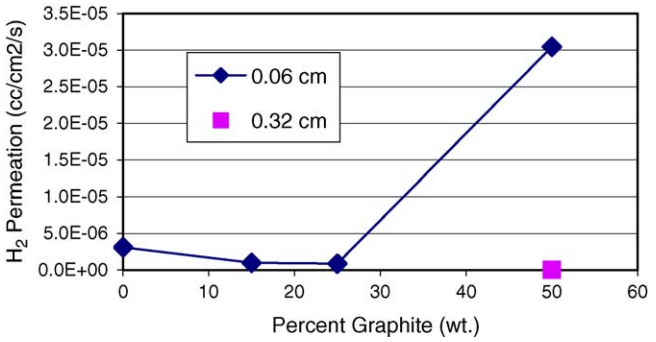

Fig. 10. Effect of graphite concentration on the H_2 permeation rate (UCAR/Hylar material).

H_2 permeation results are plotted in Fig. 10. At 172 kPag pressure (H_2 and Ar) and 0.06 cm thickness, the permeation rate goes through a minimum as graphite loading increases, in agreement with the proposed mechanism illustrated in Fig. 2. The samples at 0, 15, and 25 w/o graphite loading exhibited diffusion-driven mass transport behavior while the 50 w/o sample exhibited convection-driven behavior, since for the latter, the H_2 permeation rate increased significantly with a reduction in Ar carrier gas pressure. However, for a thicker 0.32 cm sample at the same 50 w/o graphite, H_2 transport was low and diffusion-driven, again in agreement with the proposed mechanism. Note that the graphite concentration at the minimum permeation rate is anticipated to be lower under dry mix versus wet mix conditions because wet mixing reduces the number of voids between graphite particles, which, in turn, impedes H_2 transport.

4.3. Temperature effects

Temperature is known to affect many rate processes, particularly those involving diffusion. Increasing the temperature of a polymer results in an increase in chain segmental motion and, in turn, an increase in the rate of permeation. If the thermal energy density is sufficient, the polymer may go through glass and melt transitions, which further increase the rate of diffusion processes.

The effect of temperature on the through-plane H_2 permeation rate for composite material S is shown in Fig. 11. The material was tested at 172 kPa pressure, 100% RH, and at a sample thickness of 0.06 cm to ensure diffusion-driven permeation. As expected, the rate of permeation increases linearly

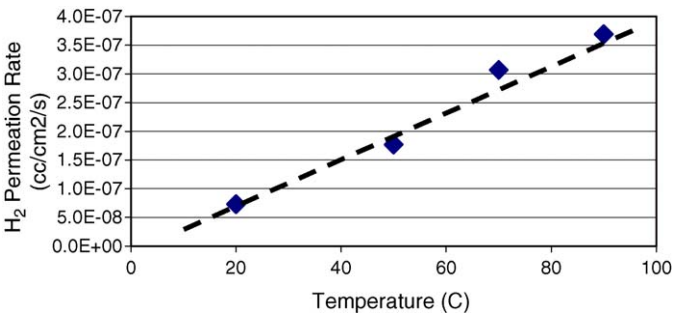

Fig. 11. Effect of temperature on the H_2 permeation rate (composite S material).

with increasing temperature. The glassy polymer (T_g = 204 °C) expands with increasing temperature (20–90 °C), thereby creating more free volume due to increased segmental motions. Only near or above the T_g would one expect an exponential increase in the permeation rate with increasing temperature, but, of course, this will not be realized in a PEM fuel cell operating at a maximum temperature of approximately 90 °C.

Note that the presence of sorbed penetrant (e.g. fuel cell product water or coolant) also increases the free volume in polymers. If the solution process is ideal, with no volume change of mixing, the change in system free volume with increasing penetrant concentration will be proportional to that obtained by an increase in temperature. Temperature-concentration superposition principles have been developed to predict simultaneous effects of temperature and penetrant concentration on diffusion processes.

4.4. Aging effects

Composite plates must survive mechanically, chemically, and electrochemically for 10 years in the aggressive fuel cell environment. For the most part, the graphite and polymer ingredients in composite plate materials are electrochemically inert under both anodic and cathodic fuel cell conditions, and the materials contain little, if any, contaminants that may leach out and adversely affect the electrode or membrane performance. However, there is great concern on whether composites will be mechanically stable at stack operating conditions (e.g. 90 °C, 100% RH, 1.4 MPa compression), particularly at a desired web thickness of only 0.03 cm.

Polymers are known to age both physically and chemically, resulting in a decrease in mechanical properties and, in turn, a potential increase in the H_2 permeation rate. A polymer will physically creep when subjected to mechanical loads and exposed simultaneously to heated solutions. This is especially true for thermoplastics. Creep experiments are often used for elucidating the nature of polymer chain segmental motions as they affect both viscoelastic and transport (diffusion) behaviors. Polymers will also chemically age or dissolve in a variety of solvents, including water. The net result of physical and chemical aging is the possibility of increasing the free volume needed for mass transport.

To investigate aging effects on permeation rates, composite T and S materials were soaked for 25 days in a pressure pot filled with de-ionized water at 130 °C. The samples consisted of both permeation samples (0.04 cm thick) and dynamic mechanical analyzer (DMA) samples (6.0 cm × 1.5 cm × 0.1 cm). The 130 °C water temperature is unrealistic and significantly higher than the maximum fuel cell temperature of 90 °C, but was chosen to accelerate the rate of aging so that aging trend results could be obtained in a timely manner. Note that 130 °C is well below the T_gs of composite S (204 °C) and composite T (180 °C) materials. Also, note that both of these materials were included in previous creep rupture (ASTM 2552) and flexural strength (ASTM D790) experiments performed by the authors, and tested at 90 °C for 10,000 h in ethylene glycol-based coolants and fuel-cell simulated solution (1.8 ppm HF, 12.5 ppm H_2SO_4, pH 3). Depending on the aqueous-based medium, the flexural strength for composite T and S decreased between 30 and 50% and between 5 and 10%, respectively. Composite S also performed significantly better than composite T in the creep rupture test, as shown in Fig. 12. At tensile stresses below 11 MPa, all composite T samples failed within 1000 h when soak at 80 °C in an ethylene glycol-based coolant; whereas composite S samples did not fail up to 8800 h of soaking and testing is ongoing. These results indicate conclusively that composite materials age in a fuel cell environment.

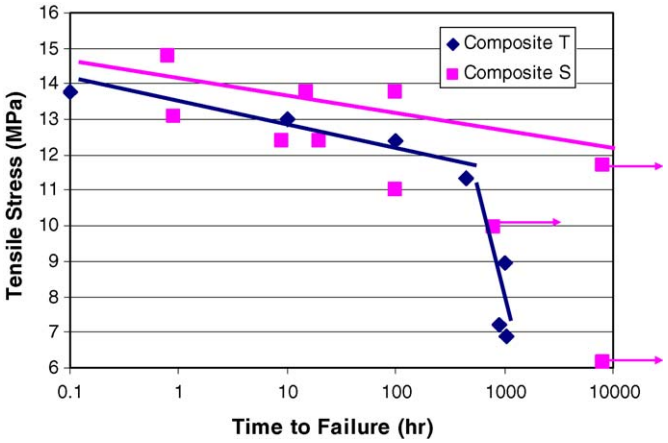

Fig. 12. Environmental stress rupture (Creep) testing of composite T and S materials in ethylene glycol-based coolant at 80 °C (arrows represent ongoing tests—samples unbroken).

Results from DMA testing are shown in Fig. 13. DMA aging measurements were conducted because DMA rheometers are highly sensitive for probing the molecular structure of polymers and they are non-destructive, thus enabling the samples to tested before and after soaking for property changes at high resolutions. A double cantilever fixture was used at 1 Hz, 13 μm amplitude, and at 25 °C. The storage moduli for the soaked (samples 1–5) composite S material decreased between 17 and 31%; whereas for the non-soaked samples (6 and 7) the moduli decreased by only 4%, indicating a significant aging effect. No testing was performed on the composite T material as the samples fell apart during soaking—a huge aging effect.

H_2 permeation rate results of the aged composite S sample are listed in Table 5. Aging in 130 °C water for 25 days increased the permeation rate by a factor of nearly 15 (172 kPa

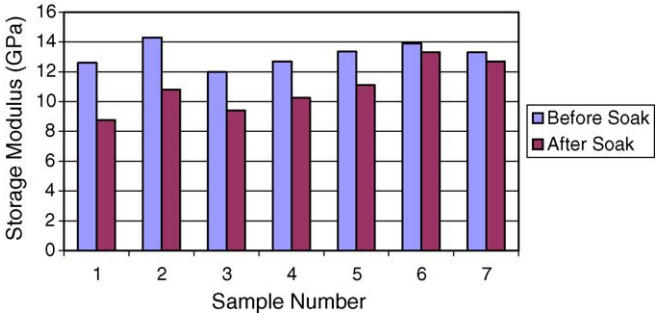

Fig. 13. Effect of aging on DMA storage modulus (composite S material): control samples 6 and 7 were not soaked.

Table 5
Effect of aging on the H_2 permeation rate (composite S material)

H_2 pressure (kPag)	Ar pressure (kPag)	Before soak permeation rate ($cm^3\ cm^{-2}\ s^{-1}$)	After soak permeation rate ($cm^3\ cm^{-2}\ s^{-1}$)
172	172	6.99 e-6	1.02 e-4
172	206	6.90 e-6	8.63 e-5
172	138	5.63 e-6	1.26 e-4
H_2 transport mechanism		Diffusion-driven	Convection-driven

H_2 and Ar pressure, 90 °C); and, simultaneously, the permeation mechanism switched from diffusion-driven (before soak) to convection-driven (after soak) mass transport. The permeation rate for the non-aged/aged sample was independent/dependent on the applied Ar pressure.

5. Conclusions/future work

High-graphite-filled composite plate materials may meet PEM fuel cell electrical conductivity targets, but unfortunately, are more likely to generate high H_2 permeation rates at the thin plate thicknesses required for high stack volumetric and gravimetric power densities. As plate thickness decreases and approaches the size of the graphite particles, the probability of a percolation network of voids forming and extending through the plate thickness increases, especially at graphite concentrations near the CPVC. Here, the mechanism of H_2 transport switches from slow diffusion to fast convection.

Composite plate suppliers currently formulate their materials at graphite concentrations slightly below the CPVC required for high electrical conductivity, high mold-filling flow capability, and adequate plate strength. H_2 permeation resistances are also high slightly below the CPVC. High permeation rate concerns arise, however, if the material is no longer homogeneous and the local graphite concentration exceeds the CPVC. This can be attributed to insufficient mixing of the wet ingredients and/or to graphite/polymer phase separation at the high shear rates generated during mold fill. Also, concerning is the fact that thermoplastic and thermoset plate materials age in the fuel cell environment, opening up the polymer structure and increasing its free volume for increased permeation.

Future studies need to further address factors affecting the H_2 permeation rate, including sanding, graphite particle size and distribution, graphite orientation, fuel-cell aging, and various compounding and molding parameters. It is strongly recommended that these studies be conducted on samples obtained from representative-sized molded plates to better investigate possible material inhomogeneity, orientation, and molding effects.

References

[1] J. Larminie, A. Dicks, Fuel Cell Systems Explained, John Wiley & Sons, New York, 2000.
[2] D.P. Davies, P.L. Adcock, M. Turpin, S.J. Rowen, Stainless steel as a bipolar plate material for solid polymer fuel cells, J. Power Sources 86 (2000) 237–242.
[3] R. Hornung, G. Kappelt, Bipolar plate materials development using Fe-based alloys for solid polymer fuel cells, J. Power Sources 72 (1998) 20–21.
[4] M.H. Fronk, R.L. Borup, B.K. Brady, S.J. Hulett, Corrosion resistant contact element for a PEM fuel cell, United States Patent Application 09/456,478 (filed: 7 December 1999).
[5] D.N. Busick, M.S. Mahlon, Los Alamos National Laboratory USA, Fuel Cells Bull. No. 5, Feburary 1999.
[6] E.K. Sichel, Carbon Black-Polymer Composites, Marcel Dekker, New York, 1982.
[7] X.S. Yi, G. Wu, D.J. Ma, Property balancing for polyethylene-based carbon black-filled conductive composites, Appl. Polym. Sci. 67 (1998) 131.
[8] A. Malliaris, D.T. Turner, Influence of particles size on the electrical resistivity of compacted mixtures of polymeric and metallic powders, J. Appl. Phys. 42 (2) (1971).
[9] R. Tchoudakow, O. Breuer, M. Narkis, Conductive polymer blends with low carbon black loading: polypropylene/polyamide, Polym. Eng. Sci. 36(10) (1996).
[10] M. Zhang, W. Jia, X.J. Chen, Influences of crystallization histories on PTC/NTC effects of PVDF/CB composites, Appl. Polymer. Sci. 62 (1996) 743.
[11] R.H.J. Blunk, C.L. Tucker, Y. Yoo, D.J. Lisi, Fuel cell separator plate having controlled fiber orientation and method of manufacture, US 6,607,857 B2, August (2003).
[12] J.C. Grunlan, W.W. Gerberich, L.F. Francis, Lowering the percolation threshold of conductive composites using particulate polymer microstructure, J. Appl. Polym. Sci. 80 (2001) 692–705.
[13] M. Abd Elhamid, R.H.J. Blunk, Y.M. Mikhail, D.J. Lisi, Separator plate for PEM fuel cell, United States Patent Application USSN 03272199 (filed: 9 July 2003).
[14] J.O. Wilkes, Fluid Mechanics for Chemical Engineers, Prentice Hall, 1999.
[15] R.H.J. Blunk, M. Abd Elhamid, Y. Mikhail, D. Lisi, Low contact resistance PEM fuel cell, US 6,811,918 B2, November (2004).
[16] J. Comyn, Polymer Permeability, Elsevier Applied Science, 1985.